Desalination and Water Treatment
www.deswater.com

doi: 10.5004/dwt.2017.20477

67 (2017) 300–308
March

Photocatalytic activity of synthesized titanate nanotubes and nanoribbons vs. commercial TiO_2 under artificial solar and visible irradiation using 17β-estradiol as model micropollutant

Ivana Grčić[a,*], Ivan Brnardić[b], Dragana Mutavdžić Pavlović[a], Vilko Mandić[a], Sanja Papić[a]

[a]*Faculty of Chemical Engineering and Technology, University of Zagreb, Marulićev trg 19, 10000 Zagreb, Croatia, Tel. 0038514597124; email: igrcic@fkit.hr*
[b]*Faculty of Metallurgy, University of Zagreb, Aleja narodnih heroja 3, 44103 Sisak, Croatia*

Received 16 September 2016; Accepted 20 December 2016

ABSTRACT

The aim of this study was to compare photocatalytic activity of protonated titanate nanotubes (HTiNT) and nanoribbons (HTiNR) vs. TiO_2 P25 under different irradiation conditions for degradation of selected water micropollutant (17β-estradiol, E2). HTiNT and HTiNR were prepared according to previously published method, hereby confirmed by means of the scanning electron microscopy and powder X-ray diffraction (XRD). In order to check the extent of photocatalytic activity at high E2 photolysis rates due to its absorption maximum (λ_{max} = 278 nm), reaction cell was exposed to the source of artificial solar light with enhanced UVB irradiation. HTiNT, HTiNR and commercial TiO_2 were active under both visible light and solar irradiation. In each irradiation regime, the E2 degradation followed pseudo-first-order kinetics with respect to both irradiation time and energy. The rate constant decreased with the decreasing catalyst load while increased with the increasing irradiation energy for the emissions below 400 nm. On behalf of achieved nanostructural arrays the wider bandgaps were shown for HTiNT and HTiNR. Compared with TiO_2 P25 almost three times lower rate constants for E2 degradation under visible irradiation were observed on behalf of band alignment effect of the P25. The photonic efficiencies (ζ_0) were calculated and used for quantitative comparison of HTiNT, HTiNR and TiO_2 photocatalytic activity regardless the irradiation conditions. The respective values decreased with the higher irradiation energy as related to an excess of photons available for simultaneous photolysis of E2 and its degradation intermediates.

Keywords: 17β-estradiol; Photocatalysis; Nanotubes; Nanoribbons; Photonic efficiency

1. Introduction

Heterogeneous photocatalysis offers a possibility for finding appropriate environmentally friendly solutions for problems affecting our environment. It can be applied to a variety of processes, including oxidations and oxidative cleavages, reductions, isomerizations, polymerizations etc. [1]. Heterogeneous photocatalysis is defined as a process whereby the illumination of semiconductor particles with irradiation suitable to its bandgap energy generates electron (e^-)/hole (h^+) pairs, consequently initiating redox chemistry on the surface [2]. Adsorbed H_2O and OH^- on the semiconductor surface act as electron donors, whereby •OH radicals are formed and used for further non-selective degradation of various organic pollutants. Photocatalytic oxidation is one of the noteworthy treatment processes for endocrine disrupting compounds [3,4] with reportedly high efficiency in degradation and mineralization of organic pollutants [5–7]. Titanium dioxide (TiO_2) in anatase crystalline form is more popular than other photocatalysts applied to environmental remediation due to its higher efficiency, stability and absence of toxicity [8]. However, its high charge

* Corresponding author.

recombination rate and its wide bandgap (~3.2 eV), which limits electron (e^-)/hole (h^+) pairs generation under visible irradiation, represents major drawbacks of anatase TiO_2. To overcome these shortcomings, a synthesis of titania-based materials with adjusted properties presents a challenge toward the development of photocatalytic materials with higher activity. Novel routes for preparation of solid photocatalysts follow the progress in nanotechnology resulting in the synthesis of nanomaterials (e.g., nanotubes) with defined geometry, physical and functional properties [9]. The increasing interest in novel photocatalytic nanomaterials arose from the possibility of lowering the bandgap and extending the respective activity further into visible spectra. Favorable properties of anatase TiO_2 made it the perfect example of photocatalysts; thus, many researches are focused on enhancing its favorable optical properties and photocatalytic activity. Research strategies commonly include doping of commercial or synthesized TiO_2, development of other oxides/semiconductor particles with desirable properties [10,11], or preparation of photocatalysts and composites with defined nanostructure.

In this paper we explore the photocatalytic activity of previously reported protonated titanate nanotubes (HTiNT) and nanoribbons (HTiNR), prepared by ion-exchange process from sodium titanate nanotubes (NaTiNT) and nanoribbons (NaTiNR). Protonation seemed as a reasonable step since it was reported that protonated nanotubes were more active than nanotubes with higher sodium content and the shortened bandgap brought the absorption of protonated nanotubes into the near visible region [12].

Since the detailed preparation method and respective structural and mechanical properties were reported earlier [9], successful preparation of HTiNT and HTiNR was only confirmed by scanning electron microscopy (SEM) and X-ray diffraction (XRD) hereby. Despite the promising properties of prepared series of protonated nanostructured photocatalysts, i.e., morphology, specific surface area, size etc., the same have never been checked for enhanced photocatalytic activity under different irradiation conditions. In the current study, HTiNT and HTiNR were tested for a degradation of emerging micropollutant in the environment varying the irradiation levels; the 17β-estradiol (E2) was used to assess photocatalytic activity of HTiNT and HTiNR in comparison with commercial TiO_2. E2 is the natural steroid, an endocrine disrupting hormone commonly released into aquatic environment from different sources [13]. Many recent studies reveal the presence of micropollutants in surface and groundwater, which can affect the animal or human endocrine system, causing abnormalities and even cancer [14,15]. E2 is the most potent natural estrogen [13], with the high estrogenic activity in concentrations of few ng/L [16].

The aim of this study was quantification of photocatalytic activities from studies catalysts in terms of photonic efficiency. Different irradiation regimes were applied to detach the photocatalytic activity from the direct photolysis of E2. Three sources of irradiation were used in the assembled illuminator ensuring: (i) simulated solar spectra with enhanced UVB irradiation, (ii) artificial standard solar spectra and (iii) visible light with small portion of UVA irradiation.

2. Materials and methods

2.1. Materials

The commercially available TiO_2 P25 (aeroxide® P25, Evonik, Germany) was used as received, while the HTiNT and HTiNR were prepared from the synthesized NaTiNT and NaTiNR. In order to prepare NaTiNT and NaTiNR, two mixtures of TiO_2 P25 and a 10-M solution of NaOH(aq) were heated, one at 135°C and other at 175°C under hydrothermal conditions for 72 h [17]. Protonated nanotubes and nanoribbons, HTiNT and HTiNR, respectively, were prepared from NaTiNT and NaTiNR by an ion-exchange process; NaTiNT and NaTiNR were dispersed separately in 0.1 M HCl using an ultrasonic bath. Prepared solution was stirred at a room temperature for 2 h, and the solid material was isolated by centrifugation. The entire procedure was repeated three more times. After the final round of centrifugation, collected solid material was washed on a centrifuge first with 0.1 M HCl and then with ethanol. Finally, the isolated material was dried at 100°C over night.

E2 was purchased from Sigma (Steinheim, Germany) and was of high purity grade (98%). Standard solution of E2 (0.5 mg/L) was prepared in Milli-Q water.

2.2. Characterization

Diffuse reflectance spectra (DRS) of powder samples were measured on a Perkin Elmer LAMBDA 35 UV–Vis spectrophotometer equipped with Perkin Elmer integrating sphere. Data were collected in wavelength range 200–800 nm^{-1} with 1 nm resolution. DRS are given as Kubelka-Munk function of reflectance vs. wavelength. Bandgap values were determined using Tauc plot. The HTiNT and HTiNR were checked with a Supra 35LV scanning electron microscope operating at 1 kV. The protonation was determined by using an energy-dispersive spectroscopy (EDS) mapping analysis. Samples for SEM characterization were prepared by placing the nanoparticles on a sample holder covered with a piece of double-sided carbon conductive tape. The sample particles were then carbon-coated. Diffraction data were collected using Shimadzu XRD 6000 diffractometer in the range of 10°–60° 2θ in step-scan mode with step of 0.02° 2θ and collecting time of 0.6 s.

2.3. Photocatalytic experiments

The photocatalytic activities of the prepared HTiNT and HTiNR and commercial TiO_2 were evaluated in terms of E2 degradation under solar and visible light. The prepared E2 aqueous solution of 0.5 mg L^{-1} with initial pH 6.5 was used. All experiments were conducted at pH 6.5 to maintain environmentally relevant conditions. Photocatalytic experiments were performed in the assembled illuminator with adjustable light emission (Fig. 1), consisting of a flow cell with the total reaction volume of 44 mL, peristaltic pump and irradiation source with the adjustable height surrounded with the reflective surface. Prior to irradiation, photocatalysts were suspended in E2 solution and homogenized in ultrasonic bath for 1 min and then recirculated in flow cell in the dark for 30 min to get an adsorption/desorption equilibrium. Recirculation flow rate used in all experiments was

67 mL min^{-1}. During photocatalytic experiments the flow cell was directly irradiated from the top. The sources of irradiation were: (i) full-spectrum compact fluorescent bulb simulating solar spectra with enhanced UVB irradiation, hereafter: "high UVB output" (Exo Terra, 20 W); (ii) full-spectrum compact fluorescent bulb simulating solar spectra, high color rendering Ra98/Class 1A with color temperature of 5,600 K, i.e., daylight characteristic, hereafter: "low UVB output" (Sunlight Pro 2.0, 23 W) and (iii) incandescent bulb emitting nominally visible light (Osram Daylight, 100 W). Measuring the emission from the latter the small portion of UVA irradiation with uniform intensity during reaction time span was noticed and thus will be referred as "visible – low UVA output" further on. Irradiation intensity was measured on the suspension surface with UVP UVX radiometer, fitted with the corresponding sensors. The emission spectra of the full-spectra lamps in the UVB and UVA regions were equal to the spectral response of the midrange and long wave UV sensors.

2.4. Analytical methods

The liquid chromatography analyses were performed using Varian ProStar 500 (Walnut Creek, California, USA), an HPLC system consisting of a ProStar autosampler 410, ProStar 230 tertiary pump system, ProStar 363 fluorescence (FLD) detectors and a thermostatted column compartment equipped with a Synergy Fusion-RP18 embedded column C18 (150 mm × 4.60 mm, particle size 4 μm) supplied by Phenomenex (USA). The column temperature was set to 30°C, and an injection volume of 20 μL was used in all analysis. The analysis was conducted using eluent A (0.01% formic acid in Milli-Q water) and eluent B (acetonitrile) in gradient elution mode, which started with a 4-min linear gradient from 70% A to 60% B, followed by a 3-min linear gradient to 95% B, which was maintained for 6 min and then a 0.1-min linear gradient back to 70% of A. After gradient elution, the column was equilibrated for 2 min before another injection. The flow rate was 0.5 mL/min. Detection of E2 in all samples was accomplished at an excitation wavelength of 280 nm and an emission of 310 nm. Fluorescence detector wavelengths were selected based upon literature [18]. Limit of detection and quantification of E2 for above-described method were 0.0005 and 0.001 mg/L, respectively.

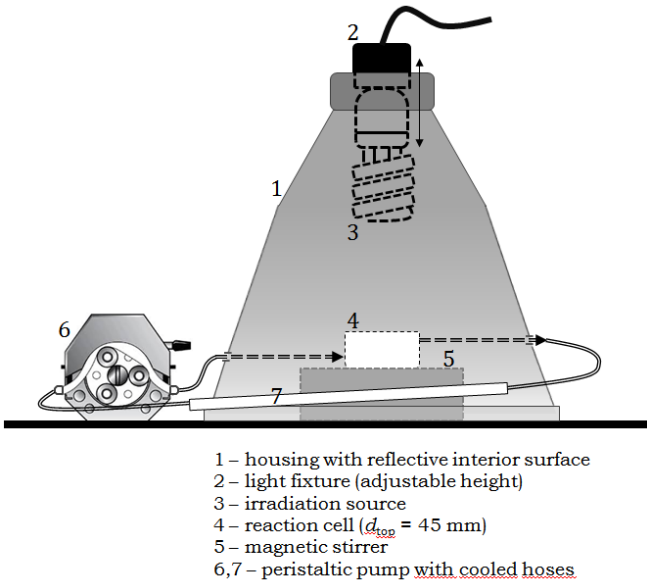

Fig. 1. Schematics of the illuminator.

3. Results and discussion

3.1. Protonated titanate nanotubes and nanoribbons

The successful preparation of nanotubes and nanoribbons was confirmed by means of the SEM and by the powder XRD (Fig. 2). Since the results were in agreement with literature [17] and our previous works [9,19], additional characterization methods were not repeated. Broad and weak diffraction peaks were observed for TiNT at approximately 10.0°, 24.8°, 28.3° and 48.3° 2θ. Obtained XRD pattern is consistent with hydrogen titanium oxide hydrate, $H_2Ti_2O_5{\cdot}H_2O$ (Joint Committee on Powder Diffraction Standards card: 47-0124) with interlayer spacing of 0.906 nm. Broadening of the diffraction peaks can be attributed to the nanometer dimensions of the tubes and also to their poor crystallinity. Sharp peaks in spectra of TiNR point at its increased crystallinity [16]. Approximate diameters of TiNT and TiNR were determined using Scherrer formula at 10 and 29 nm, respectively. As depicted by SEM imaging, TiNT have several hundred nanometers in length, while the longer dimension of TiNR was observed, reaching up to few micrometers. After consulting the available literature it was noted that the best photocatalytic activity was achieved with HTiNT [12] so the protonation of our synthesized TiNT and TiNR were performed. The protonation was confirmed by an EDS, whereby Na was not observed in studied samples (results not shown).

Observed dissimilar morphologies of TiNT and TiNR resulted also in the divergence in the respective active surface areas. The nanotubes prepared by applied method were found to have high active surface areas of about 250 m^2 g^{-1},

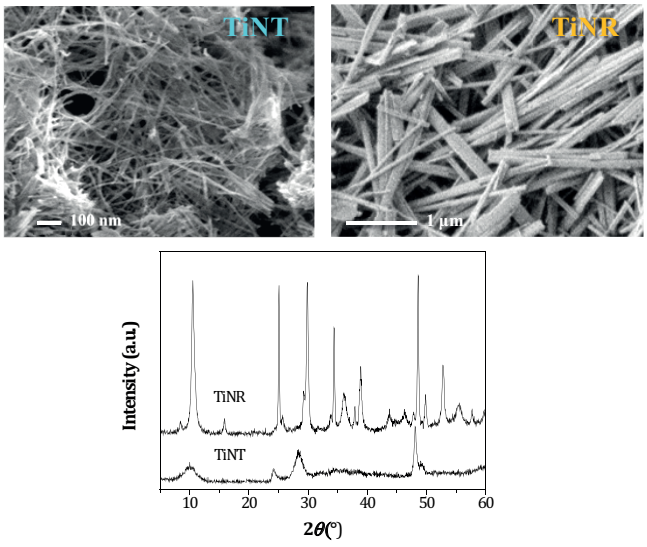

Fig. 2. Morphology of prepared TiNT and TiNR (upper figures) and powder XRD patterns (lower figure).

while nanoribbons were characterized with much smaller active surface areas of approximately 30 $m^2 g^{-1}$ [20].

DRS (Fig. 3) of prepared samples were compared with commercial untreated TiO_2 P25 powder sample in order to give additional information on favorable photocatalytic behavior of the prepared samples. To achieve more accurate analysis, two samples of each nanotubes and nanoribbons were studied (HTiNT (1), HTiNT (2), HTiNR (1) and HTiNR (2)). As given in Fig. 3, neither photocatalysts absorb in the visible region. In the UV region, all samples yield wide absorbance band centered at about 225 nm. The band is attributed to the transition electronic interband. To see whether the samples textural differences reflect in their susceptibility to behave as catalysts, it is necessary to observe the bandgap, i.e., the energy difference between the top of the valence band to the bottom of the conduction band. For the anatase bandgap, literature offers value of 3.23 eV. It is generally accepted that electron transition resembles indirect type for TiO_2 samples composed mainly of anatase; however, direct electron transitions may be considered depending on the type of preparation method and particle sizes of anatase [21,22].

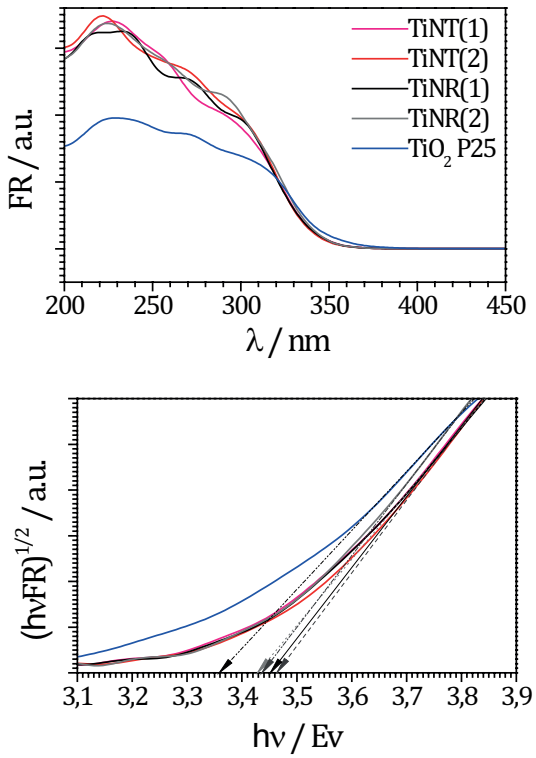

Fig. 3. DRS (Kubelka-Munk) spectra (top) and Tauc plot with bandgap results for indirect electron transitions (bottom).

The bandgap values were found as the intercept of the linear portion on the Tauc plot (indirect transitions given in Fig. 3). Table 1 shows calculated bandgap values for both indirect and direct transitions. Bandgap values derived from indirect electron transitions are more acceptable whereas TiO_2 P25 resembles the lowest values of about 3.36 eV. As previously stated commercial titania P25 consist of anatase and rutile, former usually display bandgap of ~3.2 eV while second ~3.0 eV. While pure anatase bandgap has been elaborated extensively, the lack of observation of rutile bandgap should be clarified. Surface-sensitive method like UV spectroscopy will have limited access to activated rutile electrons (based on the rutile particles lower specific surface), especially as they are known to display high bulk recombination susceptibility (while anatase yields low bulk recombination susceptibility) [23]. Therefore, only a minor effect can be expected on behalf of rutile bandgap contribution, not sufficient for Tauc plot. On the other hand, another reason for the lack of rutile bandgap can arise as a consequence of composition of P25 poor on rutile and especially anatase–rutile interface interaction. Theoretically, the thermodynamics aspects (crystallographic unit cell) as well as the number of repeating units (particle size) and distribution (microstructure) will determinate the stability, i.e., bandgap of the phase. In practice, more contributions will attribute to this matter. Major effects may arise as a consequence of interface distribution, i.e., the distribution of the anatase–rutile boundary. Therefore, the material can yield single anatase bandgap as an actual consequence of both anatase- and rutile-based charge transfer synergetic effect; the effect can be considered as energetic alignment of the band edges of anatase and rutile [24]. Such distribution in P25 can facilitate the material photoactivity as it was already reported, without affecting the bandgap value [25]. Consequently, it is reasonable to discuss only "anatase" bandgap value whereas the former actually may resemble synergetic bandgap. On the other hand, microstructural features like nanotubes and nanorods will affect the bandgap value.

Despite favorable size, well-defined nanostructure and high specific surface area of prepared HTiNT, the premise is that its wider bandgap would affect its photocatalytic activity and the latter would not reach the activity of commercial TiO_2. Even though TiNT and TiNR were extensively studied in previous works in terms of their morphology and structural properties, bandgaps were not given previously. It should be generally noted that robust preparation method and desirable structural properties and nanoscaled size of tentative photocatalysts may mislead. Refined properties, such as respective bandgap energy or optical properties, must be taken into account prior to the application for photocatalytic remediation.

Table 1
Calculated bandgaps

Photocatalyst bandgap	Nanoparticles	Nanotubes		Nanoribbons	
	TiO_2 P25	HTiNT (1)	HTiNT (2)	HTiNR (1)	HTiNR (2)
Direct	3.68	3.74	3.75	3.75	3.73
Indirect	3.35	3.45	3.46	3.43	3.44

3.2. Photocatalytic degradation of E2

The degradation of E2 was studied under different irradiation regimes in the illuminator using light sources with various emission output. Results for photolytic cleavage of E2 are shown in Figs. 4(a) and (b). Results are given as normalized E2 concentration vs. irradiation time (Fig. 4(a)) and total useful irradiation energy flux (Fig. 4(b)).

The total useful irradiation energy flux (E_{total}) can be calculated from the incident photon fluxes (I, W m^{-2}) in UVA and UVB region (290–400 nm; Eq. (1)). The incident photon fluxes were measured by radiometer over a wavelength range corresponding to UVA and UVB, and calculation was simplified to Eq. (2).

$$E_{total} = \int_0^t \int_{290nm}^{400nm} I(\lambda, t)\, d\lambda\, dt \quad (1)$$

$$E_{total} = E_{UVA} + E_{UVB} = \int_0^t I_{UVA}(t)\, dt + \int_0^t I_{UVB}(t)\, dt \quad (2)$$

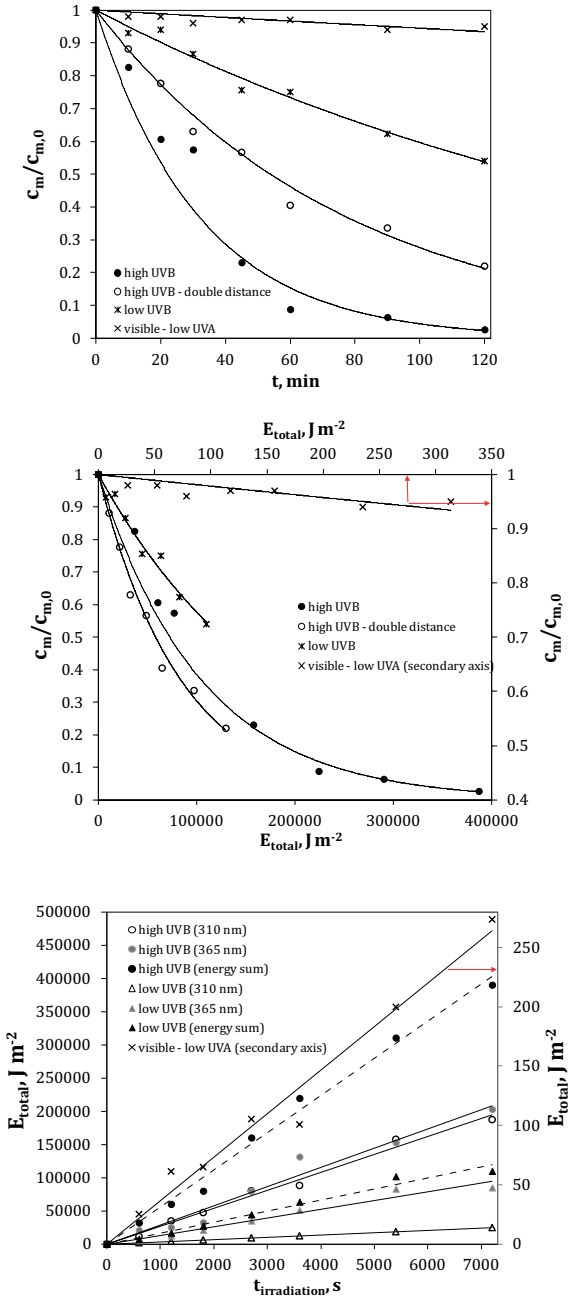

Fig. 4. (a) Photolytic degradation of E2 under different irradiation regime vs. irradiation time; (b) total irradiation energy per square meter and (c) irradiation energy vs. time.

Due to the uniform radiant incidences measured during the time span in case of each light source, it can be noticed that E_{total} increases with time linearly (Fig. 4(c)), and the transformation of reaction rate from time to energy dependent is straightforward. It is important to notice that photocatalytic rates strongly depend on the intensity of applied irradiation and it must be included in kinetic study. Normally, kinetics is presented as a function of time, but irradiation intensity over reaction time can differ greatly. In this study, total energy flux was proportional to time, and the analysis was straightforward. Sometimes, intensity may vary due to lamp lifetime or changes in electric current, which might pass unnoticed. Monitoring of light intensities and showing kinetic data dependent on photon energy flux are highly encouraged to avoid bad experimental data. The latter is even more important when dealing with natural solar irradiation when irradiation conditions vary from hour to hour, depending on the geographic location, weather etc.

The kinetics of E2 photolysis follows a pseudo-first-order rate respective to applied irradiation as follows: high UVB output > high UVB output with the source adjusted at double distance > low UVB > visible – low UVA output. Observed results correspond well with the ones found in literature [13]. Rate of photolysis is estimated at 9.42 × 10^{-6} and 5.10 × 10^{-6} m^2 J^{-1} in case of high and low UVB output, respectively. These values are used for the calculation of photonic efficiencies as explained later on. The photolysis of E2 under visible irradiation was considered negligible.

The photocatalytic activities of prepared HTiNT and HTiNR in comparison with commercial TiO_2 were studied taking into account catalyst load and irradiation effects. Results are given in Figs. 5 and 6. Normally reported higher catalyst concentration of 1 g L^{-1} resulted in instantaneous degradation of E2 over irradiated TiO_2 P25 (Fig. 5(a)). With 1 g L^{-1} HTiNT and HTiNR, E2 degradation reached 99% after 30 min of irradiation (data not shown graphically). Concentration of catalyst of 0.04 g L^{-1}, i.e., 10 times lower than that the common concentration of 0.4 g L^{-1}, which is given as optimal catalyst load in many studies, resulted in no degradation extent other than the one obtained with photolysis alone (Fig. 5(a)). In this case particularly, one cannot state that no photocatalysis takes place. There is still certain amount of E2 adsorbed on catalyst surface (Fig. 5(b)), and there might be some interactions with generated •OH radicals and/or charge transfer with the holes. However, fine distribution of catalyst particles in the irradiated system contributes to the light absorption and scattering, and certain number of photons is being captured, thus unavailable for E2 photolysis. If the photon

mass balance would be studied separately for photolysis vs. absorption/scattering on catalyst surface, lower photolysis rates might be observed. For a relatively low initial E2 concentration (0.5 mg L^{-1}), catalyst concentration of 0.1 g L^{-1} was found to be optimal. Selected initial micropollutant concentration is indeed higher than the observed single micropollutant concentration in the environment, but corresponds to the overall concentration of different micropollutants found in waste streams [13]. It is worth to mention that the capacities of prepared HTiNT and HTiNR for the E2 adsorption in dark are almost two times lower than the adsorption capacity of commercial TiO_2, despite the estimated specific surface areas of 250, 30 and 56 m^2 g^{-1} for HTiNT, HTiNR and TiO2 P25, respectively. Moreover, adsorption equilibrium is achieved after 15 min of adsorption in dark (Fig. 5(b)). Adsorption was not considered to affect the E2 degradation kinetics during photocatalytic experiment.

In this study, accent was put on quantitative comparison of photocatalytic oxidation of E2 using prepared nanotubes and nanoribbons, and the respective degradation intermediates were not studied. However, during the experiments that comprised UVB irradiation, intermediates were not detected by available analytical techniques. The explanation for this might concern the fast direct photolysis of steroid intermediates. Namely, the steroid estrogens are known to be well degraded in shallow surface waters by direct photolysis under solar irradiation due to their extended high molar absorbance in 290–360 nm range [13,15,26]. These considerations can be summarized as follows:

$$\mathrm{E2} \xrightarrow{\mathrm{UVB}} \text{photoproducts E} \xrightarrow{\mathrm{UVB}} \mathrm{A} \tag{3}$$

whereby photoproducts *E* denotes intermediates with estrogenic activity (e.g., hydroxylated forms of E2 etc.), while *A* denotes other degradation by-products such as species with aliphatic rings that were not destroyed due to high stability and low molecular weight carboxylic acids [27]. Moreover, there is evidence that intermediates formed during photocatalytic oxidation of E2 have no estrogenic effect, and that oxidation of E2 and removal of estrogenic activity occur simultaneously [28,29]. In addition to direct photolysis of photoproducts E, further hydroxylation of intermediates could contribute to a decrease in estrogenic activity by increasing hydrophilicity of the molecule, since the partly hydrophobic structure of E2 molecule is responsible for the interaction with the estrogen receptor [28]. These findings go well with the scheme given in Eq. (3), and photocatalytic treatment of water polluted with steroid estrogens seems promising. In future studies, more attention should be focused on intermediates estrogenic activities since reaction intermediates differ depending on the treatment process and intervention in the catalyst structure could greatly influence the outcome.

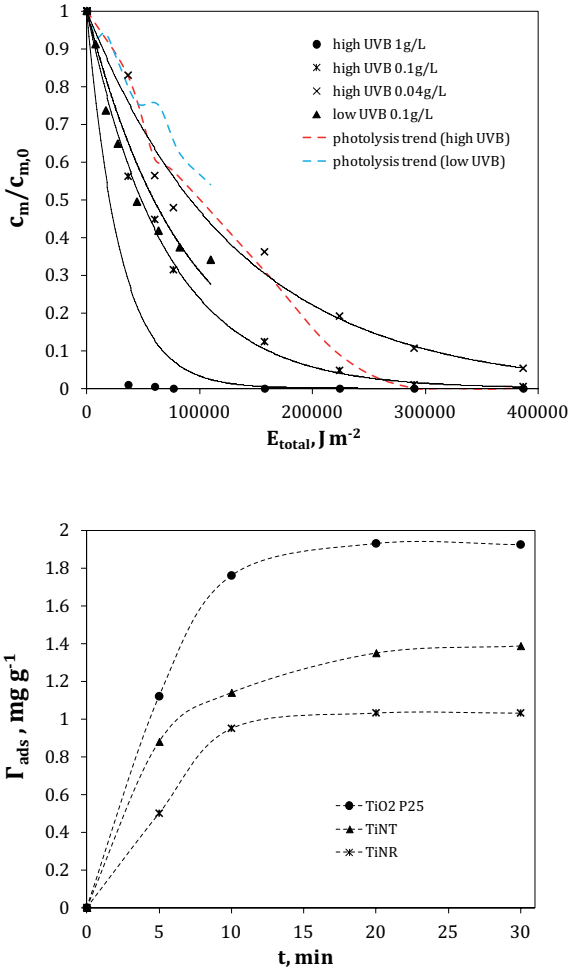

Fig. 5. (a) Photocatalytic degradation of E2 using different loads of TiO_2 P25 and (b) kinetics of E2 adsorption on the surface of TiO_2, HTiNT and HTiNR (each 0.1 g L^{-1}) in dark during 30 min.

3.3. Quantification of photocatalytic activity

All studied catalysts showed photocatalytic activity under applied irradiation regimes (Fig. 6). Kinetics of E2 degradation follows a pseudo-first-order reaction rate. In order to compare different experiments in terms of photocatalytic efficiency of studied catalysts under applied irradiation, photonic efficiencies (ζ) were used. To calculate ζ, the mathematical approach by Bahnemann et al. [30] was utilized and slightly modified. Photonic efficiency is defined by Eq. (4):

$$\zeta = \frac{R}{\epsilon_V} \tag{4}$$

where *R* is photocatalytic degradation rate, and ϵ_V is the volumetric flux of photons (Eqs. (5) and (6)):

$$R = \frac{dc}{dt} = \frac{1}{M}\frac{dc_m}{dt} \tag{5}$$

$$\epsilon_V = \frac{A_{lh}}{V_{total}} \int I' d\lambda \tag{6}$$

In Eq. (6), A_{lh} is light-harvesting area, which was approximated to the cell top surface, given in m^2; V_{total} is the reaction

volume (m^3), and c_m is mass concentration of E2. Additionally, I' is the flux of photons in the wavelength interval ($\Delta\lambda$) per illuminated surface area and time (mol m^{-3} s^{-1}). Photonic efficiency can be easily used to interpret our results because the photon fluxes in illuminator are uniform and controlled during the entire time span. It is important to point out that light-harvesting area (A_{lh}), i.e., the cell surface is illuminated homogeneously and losses of number of photons due to absorption/scattering or reflection were not considered. Having the photon flux converted to energy flux [30], photonic efficiency is further written as Eq. (7), where E_λ is the energy of mol photons at given wavelength.

$$\zeta = \frac{V_{total}}{MA_{lh}} \frac{dc_m}{\int \frac{1}{E_\lambda} d\lambda dt} \quad (7)$$

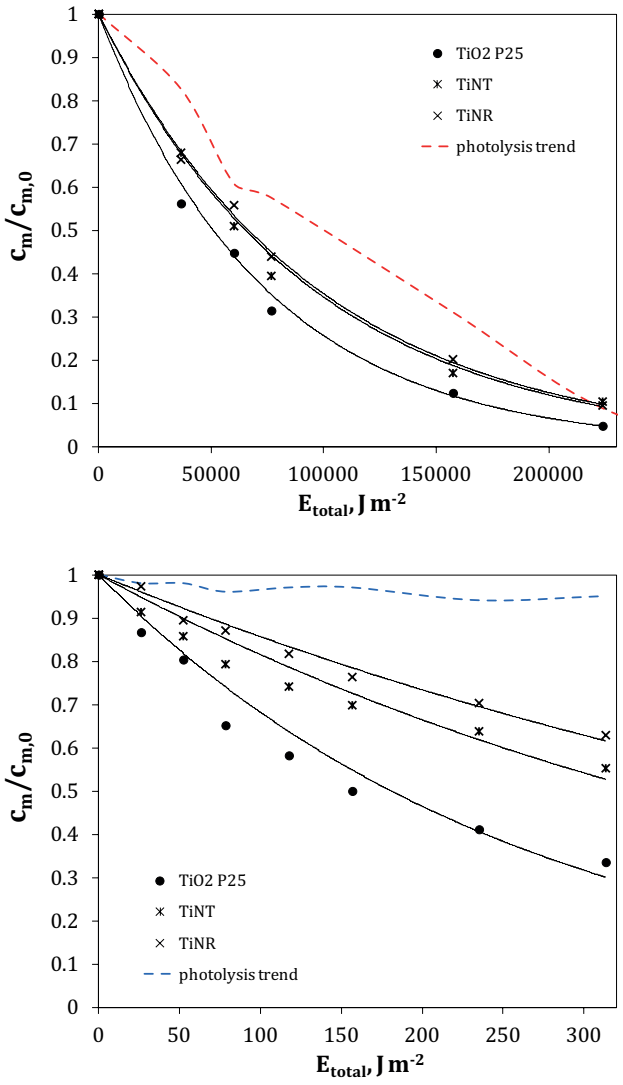

Fig. 6. Kinetics of E2 degradation using TiO_2 P25, HTiNT and HTiNR in comparison with photolysis under same conditions (catalysts load 0.1 g L^{-1}, $c_{m,0}$ = 0.5 mg L^{-1}) under (a) high UVB output and (b) visible – low UVA output.

If we assume that ζ is proportional to c_m ($\zeta = kc_m$), Eq. (7) is integrated to Eq. (8):

$$\frac{c_m}{c_{m,0}} = \exp^{-k_1 k_2 E_{total}} \quad (8)$$

with constants given as (Eqs. (9) and (10)):

$$k_1 = \frac{MA_{lh}}{V_{total}} = \frac{272.38 \times 0.0013}{4.4 \times 10^{-5}} = 8047.6 \text{ g mol}^{-1}\text{m}^{-1} \quad (9)$$

$$k_2 = k/E_\lambda = \zeta/(E_\lambda c_m) \quad (10)$$

In case where photolysis occurs parallel to photocatalysis, Eq. (8) becomes Eq. (11):

$$\frac{c_m}{c_{m,0}} = \exp^{-(k_{photolysis} + k_1 k_2) E_{total}} \quad (11)$$

Note that E_{total} (J m^{-2}) is the total photon energy per illuminated area, representing a sum of energy fluxes for UVA and UVB irradiation, given in Eqs. (1) and (2) and shown in Fig. 4(c). For both UVA and UVB part of artificial solar spectra, pseudo-monochromatic irradiation is assumed [30]; peak wavelength outputs at λ_1 = 310 nm and λ_2 = 365 nm are used for calculations, which corresponds to sensor readings and calibration Pseudo-first-order reaction rate constant for photolysis ($k_{photolysis}$) is determined experimentally.

Finally, initial photonic efficiencies can be calculated from Eq. (12), using values for speed of light, Planck and Avogadro constant.

$$\zeta_0 = E_\lambda k_2 c_{m,0} = hc\left(\frac{1}{\lambda_1} + \frac{1}{\lambda_2}\right) N_A k_2 c_{m,0} \quad (12)$$

Calculated kinetic parameters from experimental data are given in Table 2. The ζ_0' represents the observed photonic efficiency, and ζ_0 is the photonic efficiency when photolysis is excluded (Eq. (11)). Applied kinetic model fitted experimental data well with high correlation coefficients from 0.9365 to 0.9988.

Calculated ζ_0 is given for each irradiation regime and each studied catalyst at different loads. It is observed that ζ_0 decreases with decreasing catalyst load in the studied range. It is important to notice that photonic efficiencies rise as irradiation energies corresponding to UVB and UVA region decrease, meaning that the available small portions of useful photons (in case of visible – low UVA output lamp) are successfully harvested by applied photocatalysts. This observation implies that all studied photocatalysts should be efficient for outdoor applications. Furthermore, calculated photonic efficiencies (<0.005) revealed that solar irradiation possesses sufficient quanta of photons for parallel direct photolysis and photocatalytic oxidation of steroid estrogens, which is an important finding. The quantification of photocatalytic

Table 2
Kinetic data for E2 photocatalysis

Photocatalyst	Light source	Incident photon flux[a], I_{UVA}; I_{UVB}, W m^{-2}	$c_{catalyst}$, g L^{-1}	($k_{photolysis}$ + k_1k_2), m^2 J^{-1}	k_2, mol m^3 g^{-1} J^{-1}	ζ_0′	ζ_0
TiO_2	High UVB output	28.17; 26.01	1	1.00×10^{-4}	1.11×10^{-8}	0.00436	0.00394
			0.1	1.22×10^{-5}	3.46×10^{-10}	0.00054	0.00012
			0.04	7.30×10^{-6}	≈0	0.00032	≈0
TiNT			1	5.02×10^{-5}	5.07×10^{-9}	0.00223	0.00181
			0.1	1.15×10^{-5}	2.59×10^{-10}	0.00051	0.00009
TiNR			1	5.03×10^{-5}	5.08×10^{-9}	0.00223	0.00181
			0.1	1.07×10^{-5}	1.60×10^{-10}	0.00047	0.00006
TiO_2	Low UVB	11.80; 3.45	0.1	1.47×10^{-5}	1.19×10^{-9}	0.00065	0.00043
TiNT				1.31×10^{-5}	9.95×10^{-10}	0.00058	0.00035
TiNR				1.26×10^{-5}	9.32×10^{-10}	0.00056	0.00033
TiO_2	Visible – low UVA	0.04; 0.00	0.1	8.28×10^{-3}	1.03×10^{-6}	0.16863	0.16863
TiNT				3.39×10^{-3}	4.21×10^{-7}	0.06894	0.06894
TiNR				2.53×10^{-3}	3.14×10^{-7}	0.05142	0.05142

[a]Average value of radiometric readings recorded during experiments.

activity via photonic efficiency separated from photolytic phenomena presents a valuable approach for further development of solar photocatalytic systems.

Finally, despite the dissimilar morphologies and active surface areas, HTiNT and HTiNR appear to be equally efficient, while their respective photocatalytic activities observed through ζ_0 are lower than the one obtained for TiO_2 P25. These observations go in favor of the premise that perfectly shaped nanosized photocatalyst might not exhibit enhanced photocatalytic activity if the bandgap was not addressed properly. In case of artificial solar irradiation, regardless the UVB output, photocatalytic activity of HTiNT and HTiNR reached at most 90%–95% of photocatalytic activity of commercial TiO_2, but in case of visible – low UVA output, respective photocatalytic activity was about 50% lower. Except for narrower bandgap of TiO_2 P25 (Table 1), kinetic observations can be explained by specific TiO_2 P25 polymorphous structure; having an anatase and rutile in the structure results in a synergistic effect between the respective phases. As previously mentioned charge transfer may be facilitated by the band alignment. Namely the contact between anatase and rutile particle induces the transfer of •OH radicals from the surface of anatase to rutile, which serves as a sink of anatase-generated •OH radicals [31]. Consequently, new portion of •OH radicals can be generated on anatase surface, leading to higher concentrations of those species at the surface of connected dissimilar-phase particles. As shown, the kinetics of E2 degradation can be approximated with a pseudo-first-order rate, resulting from a dominant degradation mechanism via •OH radical attack [32].

4. Conclusions

In this work, HTiNT and HTiNR were prepared, and the respective photocatalytic activity was assessed based on the degradation of E2. For selected initial E2 concentration (0.5 mg L^{-1}) corresponding to approximate bulk concentration of micropollutants in waste streams, catalysts concentration of 0.1 g L^{-1} was optimal. Commonly reported optimal photocatalyst load (0.4–1.0 g L^{-1}) was unnecessarily high while no photocatalytic activity was observed at lower catalysts load (0.04 g L^{-1}).

Direct photolysis of E2 was observed due to irradiation corresponding to UVB part of artificial solar spectra. The photocatalytic activities of HTiNT, HTiNR and TiO_2 P25 were quantified and compared based on photonic efficiencies (ζ_0). Rather low photonic efficiencies ($\zeta_0 < 0.005$) were obtained when artificial solar irradiation was applied, while $\zeta_0 > 0.05$ was obtained for visible irradiation with only a small portion of UVA (I_{UVA} = 0.04 W m^{-2}). Photonic efficiencies rose as irradiation energies corresponding to UVB and UVA region decreased, leading to a conclusion that available small portions of useful photons (290–400 nm) are successfully harvested by photocatalysts, which are also active even at low UVA dosages. A tentative outdoor application of HTiNT and HTiNR for environmental remediation using sunlight is therefore confirmed.

In this work, DRS technique was applied to check direct and indirect transitions in studied photocatalyst and to determine respective bandgaps using Tauc plot. Calculated bandgaps for prepared photocatalysts were 0.1 eV wider than the one determined for commercial titania. In accordance with these findings, HTiNT and HTiNR appeared to be equally efficient, whereby respective photocatalytic activities observed through pseudo-first-order kinetic rates and ζ_0 were somewhat lower than the one obtained for TiO_2 P25. Favorable bandgap yields high overall efficiencies for HTiNT and HTiNR on behalf of nanostructural configuration while comparatively high efficiencies for P25 occur on behalf of bandgap alignment synergetic effect.

Further intervention into the structure of HTiNT and HTiNR might be required to obtain tailor-made photocatalysts with desired light absorption properties.

Acknowledgments

The authors acknowledge support of the European Commission through the COST project action No. ES1202: "Conceiving Wastewater Treatment in 2020 – Energetic, environmental and economic challenges (Water_2020)".

References

[1] J.C. Colmenares, R. Luque, J.M. Campelo, F. Colmenares, Z. Karpiński, A.A. Romero, Nanostructured photocatalysts and their applications in the photocatalytic transformation of lignocellulosic biomass: an overview, Materials, 2 (2009) 2228–2258.
[2] N. Serpone, Relative photonic efficiencies and quantum yields in heterogeneous photocatalysis, J. Photochem. Photobiol., A, 104 (1997) 1–12.
[3] Y. Wang, Y. Li, W. Zhang, Q. Wang, D. Wang, Photocatalytic degradation and reactor modeling of 17α-ethynylestradiol employing titanium dioxide-incorporated foam concrete, Environ. Sci. Pollut. Res., 22 (2015) 3508–3517.
[4] G. Li Puma, V. Puddu, H.K. Tsang, A. Gora, B. Toepfer, Photocatalytic oxidation of multicomponent mixtures of estrogens (estrone (E1), 17β-estradiol (E2), 17α-ethynylestradiol (EE2) and estriol (E3)) under UVA and UVC radiation: photon absorption, quantum yields and rate constants independent of photon absorption, Appl. Catal., B, 99 (2010) 388–397.
[5] L. Liu, Y. Li, H. Zhang, W. Zhang, Photocatalytic degradation of 17α-ethinylestradiol using ZnO self-assembly microspheres, Fresen. Environ. Bull., 21 (2012) 2232–2237.
[6] R. Fagan, D.E. McCormack, D.D. Dionysiou, S.C. Pillai, A review of solar and visible light active TiO_2 photocatalysis for treating bacteria, cyanotoxins and contaminants of emerging concern, Mater. Sci. Semicond. Process., 42 (2016) 2–14.
[7] H.S. Kushwaha, G. Parmesh, R. Vaish, K.B.R. Varma, TiO_2 microcrystallized glass plate mediated photocatalytic degradation of estrogenic pollutant in water, J. Non-Cryst. Solids, 408 (2015) 13–17.
[8] K. Mao, Y. Li, H. Zhang, W. Zhang, W. Yan, Photocatalytic degradation of 17α-ethinylestradiol and inactivation of Escherichia coli using Ag-modified TiO_2 nanotube arrays, Clean, 41 (2013) 455–462.
[9] I. Brnardić, M. Huskić, P. Umek, A. Fina, T. Holjevac Grgurić, Synthesis of silane functionalized sodium titanate nanotubes and their influence on thermal and mechanical properties of epoxy nanocomposite, Phys. Status Solidi A, 210 (2013) 2284–2291.
[10] J. Ungelenk, C. Feldmann, Synthesis of faceted β-$SnWO_4$ microcrystals and enhanced visible-light photocatalytic properties, Chem. Commun., 48 (2012) 7838–7840.
[11] J. Ungelenk, C. Feldmann, Adjustable kinetics in heterogeneous photocatalysis demonstrating the relevance of electrostatic interactions, Appl. Catal., B, 127 (2012) 11–17.
[12] V. Bem, M.C. Neves, M.R. Nunes, A.J. Silvestre, O.C. Monteiro, Influence of the sodium/proton replacement on the structural, morphological and photocatalytic properties of titanate nanotubes, J. Photochem. Photobiol., A, 232 (2012) 50–56.
[13] R.R. Chowdhury, P.A. Charpentier, M.B. Ray, Photodegradation of 17β-estradiol in aquatic solution under solar irradiation: kinetics and influencing water parameters, J. Photochem. Photobiol., A, 219 (2011) 67–75.
[14] V. Maroga Mboula, V. Héquet, Y. Andrès, L.M. Pastrana-Martínez, J. Miguel Doña-Rodríguez, A.M.T. Silva, P. Falaras, Photocatalytic degradation of endocrine disruptor compounds under simulated solar light, Water Res., 47 (2013) 3997–4005.
[15] V. Maroga Mboula, V. Héquet, Y. Andrès, Y. Gru, R. Colin, J.M. Doña-Rodríguez, L.M. Pastrana-Martínez, A.M.T. Silva, M. Leleu, A.J. Tindall, S. Mateos, P. Falaras, Photocatalytic degradation of estradiol under simulated solar light and assessment of estrogenic activity, Appl. Catal., B, 162 (2015) 437–444.
[16] E.J. Routledge, D. Sheahan, C. Desbrow, G.C. Brighty, M. Waldock, J.P. Sumpter, Identification of estrogenic chemicals in STW effluent. 2. In vivo responses in trout and roach, Environ. Sci. Technol., 32 (1998) 1559–1565.
[17] P. Umek, R. Cerc Korošec, B. Jancar, R. Dominko, D. Arcon, The influence of the reaction temperature on the morphology of sodium titanate 1D nanostructures and their thermal stability, J. Nanosci. Nanotechnol., 7 (2007) 3502–3508.
[18] Y. Yoon, P. Westerhoff, S.A. Snyder, M. Esparza, HPLC-fluorescence detection and adsorption of bisphenol A, 17b-estradiol, and 17a-ethynyl estradiol on powdered activated carbon, Water Res., 37 (2003) 3530–3537.
[19] I. Brnardić, M. Huskić, P. Umek, T. Holjevac Grgurić, Sol–gel functionalization of sodium TiO_2 nanotubes and nanoribbons with aminosilane molecules, Ceram. Int., 39 (2013) 9459–9464.
[20] P. Umek, P. Cevc, A. Jesih, A. Gloter, C.P. Ewels, D. Arčon, Impact of structure and morphology on gas adsorption of titanate-based nanotubes and nanoribbons, Chem. Mater., 17 (2005) 5945–5950.
[21] A. Welte, C. Waldauf, C. Brabec, P. Wellmann, Application of optical for the investigation of electronic and structural properties of sol-gel processed TiO_2 films, Thin Solid Films, 516 (2008) 7256–7259.
[22] D. Monllor-Satoca, R. Gomez, M. González-Hidalgo, P. Salvador, The "Direct–Indirect" model: an alternative kinetic approach in heterogeneous photocatalysis based on the degree of interaction of dissolved pollutant species with the semiconductor surface, Catal. Today, 129 (2007) 247–255.
[23] R. Kaplan, B. Erjavec, G. Dražić, J. Grdadolnik, A. Pintar, Simple synthesis of anatase/rutile/brookite TiO_2 nanocomposite with superior mineralization potential for photocatalytic degradation of water pollutants, Appl. Catal., B, 181 (2016) 465–474.
[24] D.O. Scanlon, C.W. Dunnill, J. Buckeridge, S.A. Shevlin, A.J. Logsdail, S.M. Woodley, C.R.A. Catlow, M.J. Powell, R.G. Palgrave, I.P. Parkin, G.W. Watson, T.W. Keal, P. Sherwood, A. Walsh, A.A. Sokol, Band alignment of rutile and anatase TiO_2, Nature Materials, 12 (2013) 798–801.
[25] R. Lopez, R. Gomez, Band-gap energy estimation from diffuse reflectance measurements on sol–gel and commercial TiO_2: a comparative study, J. Sol-Gel Sci. Technol., 61 (2012) 1–7.
[26] R.R. Chowdhury, P. Charpentier, M.B. Ray, Photodegradation of estrone in solar irradiation, Ind. Eng. Chem. Res., 49 (2010) 6923–6930.
[27] Y. Lin, Z. Peng, X. Zhang, Ozonation of estrone, estradiol, diethylstilbestrol in waters, Desalination, 249 (2009) 235–240.
[28] Y. Ohko, K.I. Iuchi, C. Niwa, T. Tatsuma, T. Nakashima, T. Iguchi, Y. Kubota, A. Fujishima, 17β-Estradiol degradation by TiO_2 photocatalysis as a means of reducing estrogenic activity, Environ. Sci. Technol., 36 (2002) 4175–4181.
[29] E.J. Rosenfeldt, P.J. Chen, S. Kullman, K.G. Linden, Destruction of estrogenic activity in water using UV advanced oxidation, Sci. Total Environ., 377 (2007) 105–113.
[30] D. Bahnemann, R. Dillert, J. Dzengel, R. Goslich, G. Sagave, H.-W. Schumacher, Field studies of solar water detoxification using non light concentrating reactors, J. Adv. Oxid. Technol., 4 (1999) 11–19.
[31] R. Kaplan, B. Erjavec, A. Pintar, Enhanced photocatalytic activity of single-phase, nanocomposite and physically mixed TiO_2 polymorphs, Appl. Catal., A, 489 (2015) 51–60.
[32] J. Krýsa, G. Waldner, H. Měšťánková, J. Jirkovsky, G. Grabner, Photocatalytic degradation of model organic pollutants on an immobilized particulate TiO_2 layer: roles of adsorption process and mechanistic complexity, Appl. Catal., B, 64 (2006) 290–301.